AUTOMATIC SEGMENTATION OF CORONARY ARTERIES USING BAYESIAN DRIVEN IMPLICIT SURFACES

*Yan Yang, Allen Tannenbaum, Don Giddens**

Department of Biomedical Engineering
Georgia Institute of Technology
Atlanta, GA 30332, USA

Arthur Stillman

Department of Radiology
Emory University
Atlanta, GA 30322, USA

ABSTRACT

In this paper, we propose a hybrid approach for the automatic three-dimensional segmentation of coronary arteries using multi-scale vessel filtering and a Bayesian probabilistic approach in a level set image segmentation framework. The initial surface of the coronaries is obtained from the multi-scale vessel filter response, and the surface then evolves to capture the exact boundary of the coronaries according to an improved evolution model of implicit surfaces. In our model, the image force and the propagation terms are re-defined using posterior probabilities obtained via Bayes' rule in order for the surface to approach to the boundaries faster and stop at the boundaries more accurately. The proposed method is tested on seven CT angiography (CTA) data-sets of left and right coronary arteries, and the quantitative comparison of our result against manually delineated contours on two of the data-sets yields a mean error of 0.37mm.

Index Terms

3D Image Segmentation, Level Sets, Blood Vessels, CTA

1. INTRODUCTION

Cardiovascular disease (CVD) is the most prevalent cause of death in the United States, and among the various types of CVDs, coronary heart disease accounts for the largest percentage (53%) as reported by American Heart Association [1]. Imaging techniques, such as X-ray angiography, MR angiography, and CTA have greatly assisted the diagnosis of coronary heart disease by imaging coronary arteries in living patients. Viewing and navigating through the images, however, becomes a laborious task. For each patient imaged, a large number of 2D images (e.g. over 200 slices for CTA) are needed to include the complete coronary tree. The complex shape of the coronaries also poses difficulties for one to visualize the 3D shape by looking at the 2D slices or to make measurements directly from the 2D slices. A maximum intensity projection (MIP) will not in general provide a satisfying visualization, since in CTA images, not only the coronary arteries appear in high intensity, but other blood-filled regions as well. Efficient image segmentation algorithms are essential for the isolation and visualization of coronary arteries. Once a segmentation is achieved, coronaries can be visualized as 3D surfaces, and various measurements can be performed conveniently in a 3D sense.

There have been many algorithms proposed for the segmentation of curvilinear structures in 3D; see [8] for a comprehensive survey of these methods. We mention here two of the most popular approaches: parametric (e.g., [15]) and geometric (e.g., [2]) deformable models. While many times giving satisfactory results, there are nevertheless some problems with these techniques. For example, parametric deformable surfaces do not directly allow topological changes, and the geometric or level set approach is computationally expensive. Conventional deformable models also suffer from leakage at places where the intensity gradients of the edges are relatively weak, and are very sensitive to the placement of the initial contour of the propagating front. A number of methods have been investigated to help alleviate these problems. For example, vessel filters [6, 11] can be used to enhance curvilinear structures in 3D and suppress other types of structures; local shape constraints [10] and front freezing methods [5] have been used in the level set framework to discourage leakage. These techniques, however, do not address the problem with the image force, which sometimes leads to a narrowed segmentation of vessels [9] when intensity gradients are the only measure used for the force.

We propose a hybrid approach that incorporates Bayesian posterior probabilities into the level set segmentation framework by defining a new image force term that provides better defined valleys for the values at the boundaries in order to stop the evolving surface. This prevents the undesired result

*This work was supported in part by grants from NSF, AFOSR, ARO, MURI, MRI-HEL as well as by a grant from NIH (NAC P41 RR-13218) through Brigham and Women's Hospital. This work is part of the National Alliance for Medical Image Computing (NAMIC), funded by the National Institutes of Health through the NIH Roadmap for Medical Research, Grant U54 EB005149. Information on the National Centers for Biomedical Computing can be obtained from http://nihroadmap.nih.gov/bioinformatics.

of narrowed vessels when using image terms based on intensity gradients. An adaptive propagation term that allows the surface to change its propagating direction is also proposed using posterior probabilities to effectively prevent leakage. A multi-scale vessel filter is applied to eliminate structures with the same intensity as the coronaries but without a vessel-like shape. From the filter response we also obtain the initial surface for the level set segmentation.

2. METHODS

We refer the reader to the texts [12, 13] for extensive treatments (and references) of level set methods and their use in image segmentation. In this section, we very briefly review some of the relevant facts.

We accordingly start with the classic formulation of level set flow used in image segmentation:

$$\frac{\partial \Psi}{\partial t} + F|\nabla \Psi| = 0, \tag{1}$$

where $\Psi(x, y, z, t)$ is the level set function (usually initialized via a signed distance function) with zero level-set representing the implicit 3D surface, t is an artificial time parameter (which in certain cases represents a gradient descent parameter), and F is a scalar speed function usually depending on local curvatures κ, propagation force ν and image stopping term ϕ: $F = -\phi(\nu + \kappa)$.

With the usual choice of these terms, ν represents a unidirectional constant inflationary force, and $\phi = \frac{1}{1+\|\nabla G_\sigma * I\|^2}$ where G_σ is a Gaussian filter with standard deviation σ and I is the image intensity function. Unfortunately this classic level set method and its many variations fail to segment coronary arteries. The major problems are leakage and narrowed vessels; see Figure 1(a) for a 2D example. In order to achieve a successful and accurate segmentation, we incorporate Bayesian posterior probabilities into the level set segmentation framework to construct a new image term and an adaptive propagation term for the segmentation of coronary arteries.

2.1. Bayesian Driven Image Term and Adaptive Propagation Term

We first calculate the Bayesian posterior probabilities of the voxels within the volume of interest [7] as follows:

$$Pr(\mathbf{x} \in c_k | I(\mathbf{x}) = i) = \frac{Pr(I(\mathbf{x}) = i | \mathbf{x} \in c_k) Pr(\mathbf{x} \in c_k)}{\sum_\gamma Pr(I(\mathbf{x}) = i | \mathbf{x} \in \gamma) Pr(\mathbf{x} \in \gamma)}. \tag{2}$$

This means that given the probability density function $p(I(\mathbf{x})|c_k)$ of each image class c_k and the prior probability $Pr(\mathbf{x} \in c_k)$ of each class, posterior probabilities can be calculated via the Bayes' rule (2) in order to give the probabilities of a single voxel at position $\mathbf{x} = (x, y, z)$ belonging to different classes.

In this preliminary work, the prior probability $Pr(\mathbf{x} \in c_k)$ is chosen to be $1/n$ (n is the total number of classes) to impose equal weights on all the classes. A Gaussian mixture model (GMM) is used to approximate to histogram of the images, in order to provide the probability density function for each class. Note that the noise property of CT images makes GMM a natural choice for this purpose. If other types of images such as ultrasound images are of interest, other functions in addition to the Gaussian should be considered in order to achieve a better approximation. We use the expectation maximization (EM) method to estimate the mean and standard deviation of the Gaussian function for each class. The EM procedure is initialized with a k-means clustering of downsampled voxels within the volume of interest.The posterior probabilities are then anisotropically smoothed using an affine invariant 3D filter as in [14] in order to reduce noise.

We now construct the image stopping term from the posterior probabilities obtained as above. Suppose we have a bimodal image with class c_{in} representing the object to be segmented, and class c_{out} representing the background. We then define the image stopping term as the squared difference between the posteriors that voxel $\mathbf{x}$ belongs to c_{in} and c_{out}:

$$\phi(\mathbf{x}) = (Pr^*(\mathbf{x} \in c_{in}) - Pr^*(\mathbf{x} \in c_{out}))^2, \tag{3}$$

where Pr^* is the smoothed version of the posterior probability using the anisotropic filtering. This can be easily extended to n classes ($n > 2$) by using the squared difference between the largest two posterior probabilities for the current voxel. Figure 1 (b) & (d) compare the image term based on gradients and the one based on posterior probabilities. It can be easily seen that the newly proposed image term provides a better defined dark valley at the boundaries, and within a homogeneous region, it has a smooth large value that allows the surface to propagate faster.

In order to define an adaptive inflationary term, we first use the *maximum a posteriori* (MAP) rule to obtain a classification for each voxel:

$$C(\mathbf{x}) = \arg \max_{c \in \{c_{object}, c_1, \ldots, c_{n-1}\}} Pr^*(\mathbf{x} \in c | I(\mathbf{x}) = i), \tag{4}$$

where $C(\mathbf{x})$ is the class to which voxel $\mathbf{x}$ belongs. The function ν can then be defined (for $k_1, k_2 > 0$) as follows:

$$\nu(\mathbf{x}) = \begin{cases} -k_1 & \text{if } C(\mathbf{x}) = c_{object}, \\ +k_2 & \text{if } C(\mathbf{x}) = c_{other}. \end{cases} \tag{5}$$

This means that when the current surface has a higher probability of being inside the object at a certain voxel, the propagation term will force the surface to expand, and when the surface has a higher probability of being outside of the object, this term will force it to shrink. The adaptive propagation term effectively prevents leakage, and because there is

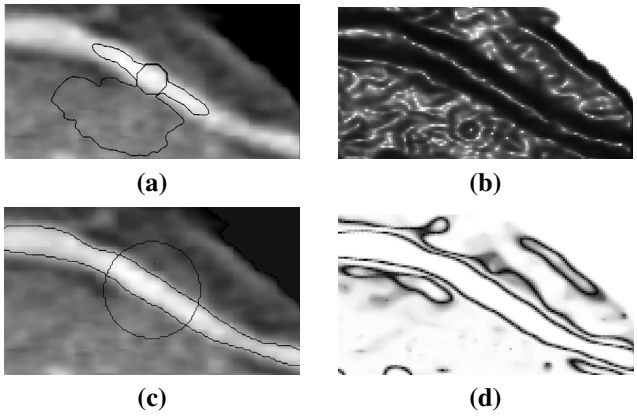

Fig. 1. Comparison of the segmentations using the conventional level set method and the proposed method; circles in (a) & (c) are initial contours. (a). Leakage and narrowed segmentation occur in the result of the conventional method; (b). Image stopping term based intensity gradients, used for generating (a). Darker region indicates lower values; (c). Successful segmentation achieved using the proposed method; (d). Image stopping term based on Bayesian posterior probabilities, used for generating (c).

an extra force to pull the contour back if it should leak, k_1 can be set to a larger constant than in the conventional active contour model to inflate the surface with larger force. This helps to reduce the total number of iterations and thus reduce the computational cost. Figure 1(c) shows the result of successfully segmenting a 2D vessel using the proposed image term and adaptive propagation term. Here we compared our results only with the conventional edge based method since they both have an edge map generated during the segmentation process. There exist many other segmentation methods, such as the widely used region-based methods [4, 17], for which we leave possible comparisons to future work due to the length of this note.

2.2. Multi-scale Vessel Filtering for the Generation of Initial Surfaces

One of the challenges in segmenting coronaries from CTA images in 3D is that several objects such as the aorta and heart chambers are in the same intensity range as the coronaries, and as a result, starting the segmentation with an initial surface near these objects will easily lead to leakage. These objects, however, can be eliminated using shape filters since they are usually blob-like structures and have very different shape features than tube-like structures (coronary arteries). The isosurface of the vessel filter response can then serve as the initial surface for level set segmentation and significantly reduce the number of iterations as oppose to starting with a seed point.

The vessel filter is based on the analysis of the eigenvalues of the Hessian matrix of the 3D image, and the elements of the Hessian matrix can be calculated by convolving the image with the second partial derivatives of an isotropic Gaussian function with standard deviation σ_f.

The properties of the eigenvalues ($|\lambda_1| \leq |\lambda_2| \leq |\lambda_3|$) of the Hessian matrix give important information about the type of structures to which the given voxel belongs. The following condition indicates that the voxel belongs to a vessel-like structure [3]: $\begin{cases} 0 \approx |\lambda_1| \ll |\lambda_2| \leq |\lambda_3|, \\ \lambda_2 < 0, \lambda_3 < 0. \end{cases}$

In order to differentiate the vessel-like structure from other types of structures, we adopted the "vesselness" measure proposed by Frangi *et al.* [6]. This measure gives larger values for vessel-like structures and smaller values for other types of structures. The vesselness measure is calculated at different scales by using several different values of σ_f, and the final vessel filter response is obtained by selecting the largest filter response of the measure at different scales. In addition, to eliminate a false positive response of the vessel filter from vessels inside the lungs, a heart segmentation is obtained first, and only voxels within the heart are made candidates for vessel filtering.

3. RESULTS AND VALIDATION

To test the proposed method, seven data-sets imaged at different clinical sites using different CT machines were segmented for coronary arteries. For level set implementation, we used the narrow band approach to reduce computational cost.

Figure 2 lists two data-sets as examples showing the 3D segmentation results of left and right coronary trees as surfaces. It can be seen that the main coronary arteries: left main (LM), left anterior descending (LAD), left circumflex (LCX) and right coronary artery (RCA) have all been successfully extracted and visualized. Figure 2 (b) shows the segmented left coronary tree rendered with the heart. Figure 3 shows two slices of the original images overlaid with the segmentation contour. It can be seen that the coronary arteries are successfully extracted and other objects with the same intensity are left as is.

Validation is conducted in two manners. We first evaluate the method by calculating the successful vessel extraction rate on all seven data-sets. For the four main coronary arteries LM, LAD, LCX and RCA, the success rate was 100%. On the left side, our method extracted a total of four branches in 4 of the data-sets (57%), and three branches in 3 data-sets (43%). Two data-sets were then compared against expert delineated contours based on the availability of the manual segmentation. In terms of coverage rate, 89.5% and 86.3% expert delineated cross-sections of coronaries are detected and segmented by our method. All individual contours are compared against the manually drawn contours, and the average mean distance error is 0.37 mm. The average of maximum error is 1.36 mm for these two data-sets. The results of the automatic

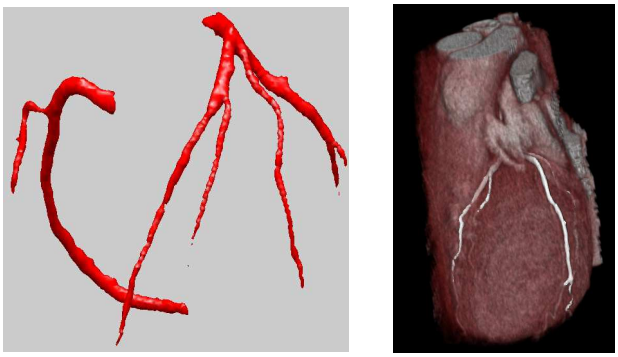

(a) (b)

Fig. 2. 3D results. (a) Left and right coronary arteries rendered as surfaces. (b) Left coronaries rendered with the heart.

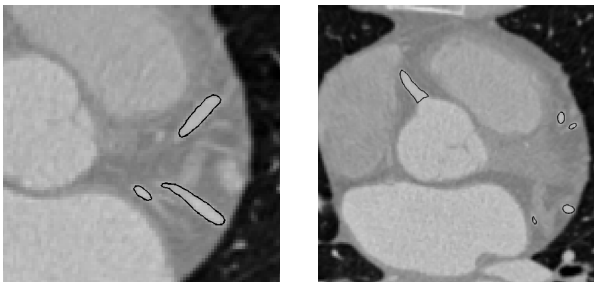

(a) (b)

Fig. 3. Segmentation results shown in 2D. (a) slice 62, and (b) slice 70 from the dataset shown in Fig. 2 (b).

approach, however, usually exhibit a much smoother appearance than the manual segmentation, especially when rendered as a surface in 3D, which means the automatic approach preserves better coherency across slices.

4. CONCLUSION AND FUTURE WORK

In this paper, we proposed an approach that segments coronary arteries from CTA images using Bayesian driven level set models and multi-scale vessel filtering. The method was tested on real clinical data and promising results were achieved.

Based on the coronary surfaces obtained in this work, more analysis may be conducted, such as generating centerlines and measuring cross-sectional radii/areas in order to detect and evaluate coronary stenosis [16]. Another possible future research direction is the segmentation and detection of soft atherosclerotic plaques in the vessel wall. The surface obtained in this work represents only the inner boundary of the arterial wall, and the volume formed by the surface represents the lumen. No information was given about the possible soft plaque, which is the most significant indicator of atherosclerosis. CTA is now capable of capturing soft plaques but with a very poor contrast. Thus, segmenting soft plaques can be an interesting and challenging problem.

5. REFERENCES

[1] American Heart Association, "A.H.A. Heart Disease and Stroke Statistics - 2006 Update", (2006).

[2] Antiga L, Ene-Iordache B, and Remuzzi A, "Computational Geometry for Patient-Specific Reconstruction and Meshing of Blood Vessels From MR and CT Angiography", *IEEE Trans. Med. Imag.*, **22** (2003) pp. 674-684

[3] Chen J and Amini A. A, "Quantifying 3-D Vascular Structures in MRA Images Using Hybrid PDE and Geometric Deformable Models", *IEEE Trans. Med. Imag.*, Vol. **23**, No. 10, (2004) pp. 1251-1262

[4] Chan T. F. and Vese L.A., "Active Contours Without Edges", *IEEE Trans. Imag. Proc.*, Vol. **10**, No. 2, (2001) pp.266-277

[5] Deschamps T and Cohen L. D, "Fast Extraction of Tubular and Tree 3D Surfaces With Front Propagation Methods", *Intl. Conf. Pattern Recognition*, (2002)

[6] Frangi A. F, Niessen W. J, Vincken K. L and Viergever M. A, "Multiscale Vessel Enhancement Filtering", *MICCAI'98*, LNCS **1496**, (1998) pp. 130-137

[7] Haker S, Sapiro G, Tannenbaum A, "Knowledge-Based Segmentation of SAR Data with learned Priors", *IEEE Tran. on Image Processing*, Vol.**9**, No. 2, (2000) pp. 299-301

[8] Kirbas C and Quek F, "A Review of Vessel Extraction Techniques and Algorithms", *ACM Comput. Surv.* **36 (2)** (2004), pp. 81-121

[9] Lorigo L. M, Faugeras O, Grimson W. E. L, Keriven R, Kikinis R. and Westin C-F, "Co-Dimension 2 Geodesic Active Contours for MRA Segmentation", in *Proc. 16th Int. Conf. Inform. Processing Medical Imaging*, ser. Lecture Notes in Computer Science, Visegrad, Hungary, June/July (1999), **1613**, pp. 126-139

[10] Nain D, Yezzi A, and Turk G, "Vessel Segmentation Using a Shape Driven Flow", *MICCAI 2004*, LNCS **3216**, (2004) pp. 51-59

[11] Sato Y, Nakajima S, Shiraga N, Atsumi H, Yoshida S, Koller T, Gerig G, and Kikinis R, "Three Dimensional Multi-scale Line Filter for Segmentation and Visualization of Curvilinear Structures in Medical Images", *Medical Image Analysis*, (1998), **2**, pp. 143-168

[12] Osher S and Fedkiw R, *Level Set Methods and Dynamic Implicit Surfaces*, Springer-Verlag, 2003.

[13] Sethian J.A., *Level Set Methods and Fast Marching Methods*, Cambridge University Press, 1999.

[14] Teo P. C, Sapiro G and Wandell B. A, "Anisotropic Smoothing of Posterior Probabilities", *Intl. Conf. on Image Processing* (1997) pp. 675-678

[15] Yim P. J, Cebral J. J, Mullick R. M, Marcos H. B, and Choyke P. L, "Vessel Surface Reconstruction With a Tubular Deformable Model", *IEEE Trans. Med. Imag.* **20**, (2001) pp. 1411-1421

[16] Yang Y, Zhu L, Haker S, Tannenbaum A, and Giddens D. "Harmonic Skeleton Guided Evaluation of Stenoses in Human Coronary Arteries". *MICCAI* (2005) LNCS **3749**, pp.490-497,

[17] Zhu S.C. and Yuille A, "Region Competition: Unifying Snakes, Region Growing, and Bayes/MDL for Multi-band Image Segmentation", *IEEE Trans. Pattern Analysis and Machine Intelligence*, Vol. **18**, No. 9, (1996) pp. 884-900